Electron Transfer Limitation in Carbon Dioxide Reduction Revealed by Data-Driven Tafel Analysis

Steven M. Brown[*,a], Michael J. Orella*[*,a], Yung Wei Hsiao[a], Yuriy Roman-Leshkov[a], Yogesh Surendranath[b], Martin Z. Bazant[a,c], Fikile Brushett[a,†]*

[a] Department of Chemical Engineering, Massachusetts Institute of Technology, Cambridge MA, 02139

[b] Department of Chemistry, Massachusetts Institute of Technology, Cambridge MA, 02139

[c] Department of Mathematics, Massachusetts Institute of Technology, Cambridge MA, 02139

* Authors contributed equally

[†] Corresponding author: brushett@mit.edu

Keywords: CO_2 reduction, Electrochemical Kinetics, Marcus-Hush-Chidsey, Bayesian inference

Abstract:

Carbon dioxide (CO_2) recycling holds promise to mitigate anthropogenic emissions and to increase the sustainability of many chemical and fuel production processes. Despite marked advances in catalyst activity and selectivity at laboratory scale, fundamental understanding of the

electrocatalytic reduction of CO_2 remains limited, resulting in great uncertainty when extrapolating data to industrially relevant reaction rates. Importantly, the predominant models apply linear Tafel extrapolation, which drastically overpredicts the current density at large overpotentials. Researchers have posited several models to explain the curvature in Tafel behavior for CO_2 reduction catalysis. Here we compare the ability of select models using Bayesian inference to explain curvature in Tafel behavior within the context of CO_2 reduction to CO catalyzed by gold surfaces. By harvesting Tafel data on gold surfaces from multiple literature sources in a variety of reactor configurations, we identify three important features common to the aggregate data on Au-mediated CO_2 reduction: (1) curvature in the Tafel plot at high overpotentials is only partly caused by mass transfer limitations; (2) the Marcus-Hush-Chidsey model for rate-limiting single-electron transfer kinetics provides the best fit to the data of the models tested; and finally, (3) the highly varied data collapse onto a single curve governed by the maximum predicted current in the electron-transfer-limited model. This analysis sets a foundation for determining more accurate activity-driving force relationships for CO_2 reduction on electrocatalytic surfaces, both improving the quality of system-level analyses and motivating further research into the underlying mechanisms of CO_2 reduction catalysis.

Introduction:

The electrochemical reduction of carbon dioxide (CO_2)[1–5] is an increasingly well-studied process with the potential to both mitigate greenhouse gas emissions[6] and provide new revenue streams through valorization efforts. In recent years, researchers have designed advanced electrocatalysts and reactors that efficiently transform CO_2[7–9] to formate,[10–13] carbon monoxide (CO),[14–18] methane,[19,20] ethylene,[21–23] and many other species of interest.[24–27] Nevertheless, the fundamental reaction pathways even for the simplest CO_2 reduction reactions remain widely debated.[14,28–39] This knowledge gap contributes to an incomplete understanding of the relationship between catalytic rate and applied driving force, which, in turn, inhibits progress towards improved catalysts, reactor designs, performance models, or technoeconomic forecasts. The classical Butler-Volmer (BV) kinetic model is used widely to relate the current density to overpotential. This model posits that the activation barrier for an interfacial charge transfer reaction varies proportionally with changes in the applied overpotential. The proportionality constant describing this relationship is the transfer coefficient, α, which is assumed to be constant across all overpotentials within the BV model.[40–43] Consequently, the BV model predicts that Tafel plots of overpotential versus the logarithm of the current will be linear over a moderate to large over-potential range, over which the reverse reaction is negligible and mass transport effects are minimal. Tafel analysis has been broadly applied to CO_2 reduction to obtain insights into reaction mechanisms or catalytic activity.

Interestingly, we have observed characteristic curvature of the Tafel data across multiple orders of magnitude of current densities, both throughout the published literature and our own experimental work. This phenomenon persists regardless of different reactor systems, reactant delivery methods, and catalyst structures, despite all investigating identical reaction chemistry.[44–51] Typically, curvature in the Tafel behavior for CO_2 reduction catalysis has been attributed to: (1)

mass transfer limitations of CO_2 at the electrode surface,[39] (2) uncompensated film resistance,[52] or (3) homogeneous reactions changing the local environment (e.g., pH, electrolyte composition, double-layer charge) of the electrolyte near the electrode surface.[39,53] When mass transfer is the rate-controlling process, the CO_2 reaction rate is limited by the flux of one or more reactants to the surface, not by the inherent kinetics of the reaction, causing a potential-independent current density plateau beyond a certain applied overpotential. These effects have been simulated using a multi-scale coupled mass-transfer and kinetic model.[39] However, this model predicts a sharp curvature of the Tafel slope which is at odds with experimental data showing a more smooth variation in Tafel slope. Transport effects have also been explicitly accounted for using rotation cone electrodes and these studies still reveal a characteristic curvature in the Tafel data for Au CO_2 reduction.[37] Film or series resistance, which is distinct from high-frequency resistance (typically 10^0-10^2 Ω cm^2), represents non-distributed ohmic loss[13,54] that can induce Tafel curvature at large current densities. Film resistances are commonly invoked in models of lithium-ion batteries, where passivating solid-electrolyte interphase films are known to spontaneously form and grow at the electrode-electrolyte interface.[55–57] However, operando spectroscopic studies provide no evidence of passivating film formation during CO_2 reduction on Au electrodes.[37] Moreover, the empirical introduction of series resistances within a BV kinetic model can mask inherent electrokinetic and quantum-mechanical contributions to the curvature of a Tafel plot.[58–60] Finally, it has been recognized that, due to the sluggishness of the CO_2 bicarbonate equilibrium, there exists a pronounced increase in local pH at the catalyst surface, which is only further exacerbated for porous catalysts and at high current densities. However, CO_2 reduction catalysis on Au has been found to be independent on the proton donor and pH environment[37,61] making this pH swing an unlikely contributor to Tafel curvature. For sufficiently high local pH values, the formation of

carbonate has been invoked as a cause of curvature in the Tafel behavior.[53] However, inclusion of this homogeneous reaction into electrochemical kinetic models of CO_2 reduction still generated non-linear scaling of reaction rate with applied overpotential. The foregoing discussion provides strong motivation for developing kinetic models of CO_2 reduction on Au that go beyond classical BV formalisms.

Although our observations and analysis are applicable to both Au and Ag[14,62–66] catalysts for the reduction of CO_2 to CO, we elected to focus only on Au catalysts because this restricted scope enables a deeper investigation of a widely studied catalyst that displays high faradaic efficiencies for CO at modest overpotentials. A representative subset of the aggregated data is shown in **Table 1**, where the relevant information for each data set is: (1) identification number used in this work, (2) the type of Au catalyst, (3) the supporting material, (4) the metal cation of the bicarbonate salt and its concentration, and (5) the reference from which the data was obtained. An analogous workup for CO_2 reduction to CO on silver (Ag) catalysts is presented in the Supporting Information, yielding comparable results. These data are plotted in **Figure 1** and exhibit the observed onset in curvature between 300 – 500 mV overpotential. Clearly, the BV model would significantly overpredict the currents observed at overpotentials beyond this range, as discussed above. Interestingly, common trends in curvature are observed irrespective of whether the data were collected on a rotating[37] or stationary electrode and common trends persist across orders of magnitude differences in the absolute currents, suggesting that neither series resistances nor mass transfer effects adequately explain the curvature.

Table 1: Literature data with Au catalyst materials used for kinetic modeling analyses. Each trace is assigned a unique numerical identifier, the catalyst form, the supporting material if applicable,

and the electrolyte composition. For additional information a reference is provided. *Unpublished data from Brown et al.

#	Au Form	Catalyst Support	M^+	$[M^+]$ / M
1[47]	Foil	–	K^+	0.1
2[48]	Functionalized	–	K^+	0.1
3[48]	Nanoparticles	Carbon Black	K^+	0.1
4[49]	Foil	–	Na^+	0.5
5[49]	Oxide-Derived	–	Na^+	0.5
6[50]	Nanoparticles	Carbon Nanotubes	Na^+	0.5
7[50]	Nanoparticles	Carbon Nanotubes Annealed at 400°C	Na^+	0.5
8[51]	Inverse Opal Films	–	K^+	0.1
9*	Nanoparticles	Carbon Black	Na^+	0.5

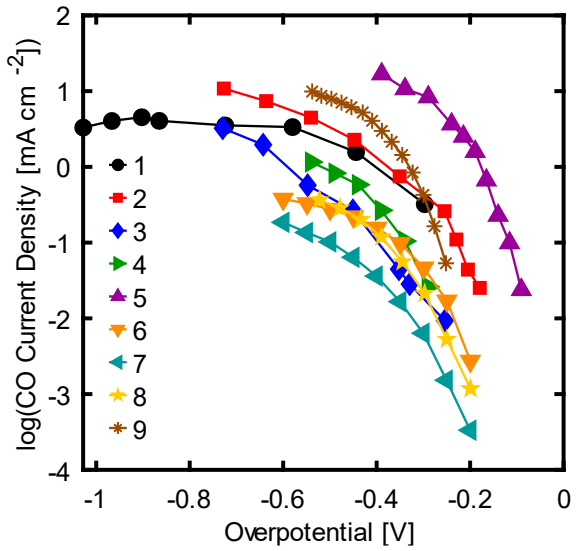

Figure 1: Tafel plot of literature data for the electrochemical conversion of CO_2 to CO on Au catalyst materials

Marcus[67–69] and Hush[70–72] developed theories to fundamentally describe both homogeneous and electrode-based outer-sphere electron-transfer reactions, where the reorganization energy is dominated by the classical electrostatic solvation energy. Around the same time, Dogodnadze, Chizmadzhev, and Kuznetsov developed the quantum-mechanical theory of electron transfer,[73–75] including inner sphere reactions, where the reorganization energy is dominated by molecular vibrations and leads to a similar mathematical form,[76–78] which provided critical insights in the fields of chemistry and biology.[77–80] For metallic electrodes, the theory predicts similar types of sublinear and/or inverted Tafel behavior, which were subsequently validated by Chidsey's experiments of electron transfer kinetics between a Au electrode and a ferrocenyl self-assembled monolayer.[41] Although the resulting Marcus-Hush-Chidsey (MHC) model has been successfully applied to electrochemical systems,[42,81] its broader application in electrochemical kinetics has lagged the classical BV model due, at least in part, to its mathematical complexity. The recent availability of simple analytical approximations[58,82] has simplified the implementation of the MHC model to fit experimental data.[59,60] Recently, CO_2 reduction data on Au has been fit to a Marcus model to extract an estimated reorganizational energy and equilibrium potential for CO_2 electrosorption.[83]

Here, we show that the MHC model effectively captures the Tafel curvature (Figure 1) observed for (inner-sphere) carbon dioxide reaction across a wide range of datasets for Au catalysts. While Marcus-type models are only strictly applicable to outer-sphere ET reactions, we take the MHC model as the best available proxy since no general analytic models currently exist that describe adiabatic inner-sphere charge transfer reactions at electrode surfaces. We describe a complete

analysis of the available models and their ability to fit the set of data mined from the literature of CO_2 reduction on Au catalysts. Our study begins by describing the individual models and then compares them based on their ability to fit the CO2RR data sets. We rely on both the physical meaningfulness of best fit parameters to qualitatively compare the proposed models and the Bayesian Inference Criterion (BIC; *vide infra*) to quantify the observed differences.[84] Rigorous quantitative analysis shows that the MHC model can be used to explain the curvature in the Tafel behavior. Through our meta-analysis, we find all of the data collapse to a common polarization curve, suggesting that CO_2 reduction on Au follows the same mechanistic pathway, regardless of catalyst morphology or electrolyte conditions. This work motives a re-evaluation of Tafel analysis to include potential-dependent changes to the transfer coefficient. More generally, our work sheds light on a challenging problem within the CO_2 reduction field and encourages more detailed investigations to elucidate underlying reaction mechanisms.

Methods:

Through this section, we present the mathematical formulations of the models and then the statistical metrics that are used to quantitatively compare any observed differences in the quality of the fits.

Electrochemical Kinetic Theories:

The ability to identify relationships between the observed reaction rate, as measured by the partial current density for CO, j, and the reaction overpotential, η, is a critical tool for analyzing electrochemical kinetics. The BV kinetic theory, shown in Equation (1), is most widely used current-potential relationship. Here j is the current density, which is positive for cathodic currents, j_0 is the exchange current density, α is the charge transfer coefficient, η is the overpotential, and

the tilde denotes normalization to the thermal voltage, where R is the universal gas constant, T is the absolute temperature (assumed constant for these reactions), n is the number of electrons transferred per mole of product formed, and F is the Faraday constant. As the elementary steps of CO_2 reduction to CO reaction remain widely debated, we performed this entire meta-analysis on the overall reaction, where the standard reduction potential is -0.10 V and two moles of electrons are transferred to produce one mole of CO. The two fitting parameters for the BV model are the charge transfer coefficient and the exchange current density.

$$j = j_0\left[\exp\left(-\alpha\tilde{\eta}\right) - \exp\left(\left(1-\alpha\right)\tilde{\eta}\right)\right], \qquad \tilde{\eta} = \eta\left(\frac{nF}{RT}\right) \tag{1}$$

As described in the introduction, reactant transport limitations may convolute the reaction kinetics. We therefore analyzed a BV model with mass transport considerations, such as CO_2 diffusion to the reaction sites. Specifically, the overpotential is partitioned (Equation (2)) between a mass transfer overpotential, η_T, which is a function of the limiting current density, j_{lim}, (Equation (3)), and the kinetic overpotential, η_K, which is normally calculated through the Butler-Volmer model (Equation (4)). In this way, the limiting current density provides an additional parameter to which the data may be fit:

$$\tilde{\eta} = \tilde{\eta}_K + \tilde{\eta}_T \tag{2}$$

$$\tilde{\eta}_T = \ln\left(1 - \frac{j}{j_{lim}}\right) \tag{3}$$

$$j = j_0\left[\exp\left(-\alpha\tilde{\eta}_K\right) - \exp\left(\left(1-\alpha\right)\tilde{\eta}_K\right)\right] \tag{4}$$

Next, to account for Marcusian deviations from the BV theory, we examined a simplified Marcus-Hush-Chidsey model developed by Zeng *et al.*(Equation (5)), which makes the kinetic prefactor, k_0, and reorganization energy, λ, calculable from fitted experimental data.[58] The kinetic prefactor scales the current response to overpotential and is directly related to the maximum achievable current density. Given that an electron transfer is nearly instantaneous relative to molecular rearrangement, per the Franck-Condon principle, for a successful electron transfer to occur, the solvating molecules must exist in an unstable state relative to an equilibrium configuration. The energy required to create these unstable states is the reorganization energy used as a fitting parameter in this model. Importantly, this model assumes a rate-limiting single electron transfer controlling the rate of the overall 2-electron CO_2-to-CO reaction. Because the equilibrium potential of the elementary charge transfer step is not known, the overpotential was calculated based on the equilibrium potential for the overall reaction. We note that calculating the overpotential in this manner will lead to an offset in the fitted reorganizational energy relative to the real value with the elementary step controlling the rate. Equation 5 assumes the reactants are in their standard states with 1M concentrations, but corrections for varying concentrations[59,60] are small in the situations without mass transfer limitation considered here.

$$j = -k_0\sqrt{\pi\lambda}\tanh\left(\frac{\tilde{\eta}}{2}\right)\mathrm{erfc}\left(\frac{\lambda-\sqrt{1+\sqrt{\lambda}+\tilde{\eta}^2}}{2\sqrt{\lambda}}\right) \quad (5)$$

As stated in the introduction, curvature in Tafel analyses has been historically accounted for by incorporating an uncompensated series resistance term into a BV model.[52,55,56] Series resistance measurements are commonplace in electrochemical cells and most modern hardware can identify and compensate for them using high-frequency impedance analysis. However, in lithium-ion batteries, uncompensated film resistances are known to develop during device operation due to

growth of a solid-electrolyte interphase film, especially at the anode.[55] In these particular devices, this uncompensated resistance is sometimes inferred to be as large as 10^2 – 10^3 ohm cm^2, albeit without any direct evidence of the film properties leading to the fitted values.[55–57] In addition, it has recently been shown that generalized MHC theory of coupled ion-electron transfer kinetics is able to fit certain data more parsimoniously than BV with a series resistance.[60] To investigate the impact that such large uncompensated resistances would have on our own models, we developed similar modifications incorporated in the "BV + R" and "MHC + R" models presented in Equation (6) and Equation (7), respectively. Internal resistance, R_{int}, is introduced in these equations making both three-parameter models.

$$j = j_0\left[\exp\left(-\alpha(\tilde{\eta}+\hat{j}R_{\text{int}})\right)-\exp\left((1-\alpha)(\tilde{\eta}+\hat{j}R_{\text{int}})\right)\right], \qquad \hat{j} = j\left(\frac{nF}{RT}\right) \tag{6}$$

$$j = -k_0\sqrt{\pi\lambda}\tanh\left(\frac{(\tilde{\eta}+\hat{j}R_{\text{int}})}{2}\right)\text{erfc}\left(\frac{\lambda-\sqrt{1+\sqrt{\lambda}+(\tilde{\eta}+\hat{j}R_{\text{int}})^2}}{2\sqrt{\lambda}}\right) \tag{7}$$

Model Fitting and Goodness of Fit:

We leveraged model fitting to solve for the best-fit parameters using the data sets presented in Table 1 to identify the most accurate model. Traditionally, updating the likelihood, p, of different models, m, relies on Bayesian inference, where some prior information about the likelihood of a given model, $p(m)$, is informed by evidence, $p(d \mid m)$, from newly collected data, d, to obtain a posterior likelihood distribution, $p(m \mid d)$. Normalization of the posterior distribution is performed by summing over all possible models, as shown in the application of Bayes' theorem, below.

$$p(m \mid d) = \frac{p(d \mid m)\,p(m)}{\sum p(d \mid m_i)\,p(m_i)} \tag{8}$$

While conceptually tractable, the model evidence, $p(d \mid m_i)$, necessary for computing the posterior distribution is only calculable by marginalizing the dependence on model parameters, $\boldsymbol{\theta}$, as shown in Equation (9). This necessitates prior distributions for the parameter values for the model of interest, $p(\boldsymbol{\theta} \mid m_i)$ resulting in a high dimensional integral that cannot be easily calculated through deterministic numerical approaches. Although stochastic methods have been developed to calculate these types of high dimensional integrals, they are sensitive to accurate integrand values.[85–87]

$$p(d \mid m_i) = \int p(d \mid \boldsymbol{\theta}, m_i)\, p(\boldsymbol{\theta} \mid m_i)\, \mathrm{d}\boldsymbol{\theta} \tag{9}$$

In the case of the CO_2 reduction specifically, and electrochemical kinetics more generally, there has been little application of Bayesian inference, and it is therefore difficult to assess the true prior distribution necessary to compute the posteriors, both for the individual models, $p(m_i)$, and for the parameters within each model, $p(\boldsymbol{\theta} \mid m_i)$. Despite this uncertainty, approximations have been developed that can be used in cases such as this, where there is significantly more data than parameters in any of the models. One such approximation is the BIC (Equation 10), which is a direct approximation of the Bayes factor by assuming large N and independent, identically distributed data.[88,89] This information criterion can be used to compare models with different numbers of fitted parameters to determine the relative likelihood that a certain model describes the observed data. Here, $\boldsymbol{\theta}^*$ are the best fit parameters which minimize the sum-squared error, N is the number of measurements, and k is the degree of the model, such that $\boldsymbol{\theta} \in \mathbb{R}^k$. With this metric, the most likely model will have the lowest BIC.

$$\mathrm{BIC}_i = \ln(N)\, k - \ln\left(\mathcal{L}_i\left(\boldsymbol{\theta}^*\right)\right) \tag{10}$$

The likelihood of a certain set of parameters, $\mathcal{L}(\boldsymbol{\theta})$, is defined as the probability of observing certain data given knowledge of those parameter values and specific model, $p(d \mid \boldsymbol{\theta}, m) = \mathcal{L}_m(\boldsymbol{\theta})$. In the case of measuring CO_2 reduction kinetics, the observed data is a deviation between the model predicted current density and the experimentally-measured current density under the same conditions. In our models, we assume that these errors are normally distributed on the log-scale, such that as the magnitude of the current increases, so too does the magnitude of the error. Therefore, the residuals for a given model ($d = \boldsymbol{\varepsilon}_m \in \mathbb{R}^N$) are defined as the difference of the log of the current (i.e., the Tafel plot differences) not simply the difference of the current (i.e., polarization plot differences), as shown in Equation (11). For this analysis, we also assume that the residuals are independent, exhibit a Gaussian distribution with zero mean, and a variance corresponding to the measurement uncertainty.

$$\boldsymbol{\varepsilon}_m(\boldsymbol{\theta}) = \log\left(\mathbf{j}_{pred,m}(\boldsymbol{\eta};\boldsymbol{\theta})\right) - \log\left(\mathbf{j}_{meas}\right) \tag{11}$$

Here, $\mathbf{j}_{meas} \in \mathbb{R}^N$ is the vector of experimental measured current densities, while $\mathbf{j}_{pred} \in \mathbb{R}^N$ is the vector of current densities predicted by using the set of kinetic parameters $\boldsymbol{\theta} \in \mathbb{R}^k$ with model m at the experimental overpotentials, $\boldsymbol{\eta} \in \mathbb{R}^N$. The likelihood of these data (Equation 12), obtained from the assumed Gaussian distribution, is shown below, where $\sigma^2 \approx 0.1$ is an estimate of the measurement variance obtained from the literature (see supplementary information).

$$p(\boldsymbol{\varepsilon} \mid \boldsymbol{\theta}, \sigma^2, m) = \mathcal{L}_m\left(\boldsymbol{\theta}\right) = \frac{1}{\left(2\pi\sigma^2\right)^{N/2}} \exp\left(-\frac{\left\|\boldsymbol{\varepsilon}_m\left(\boldsymbol{\theta}\right)\right\|^2}{2\sigma^2}\right) \tag{12}$$

To accurately fit each of the models to the data, we seek the maximum likelihood that the data would be observed given the set of kinetic parameters and experimental conditions, which will

consequently minimize the BIC for a particular model. Practically, the likelihood maximization to identify the best fit parameters, $\boldsymbol{\theta}^*$, is performed by minimizing the sum of squared residuals, as shown by Equation (13).

$$\boldsymbol{\theta}_m^* = \arg\max_{\boldsymbol{\theta}} \mathcal{L}_m(\boldsymbol{\theta}) = \arg\min_{\boldsymbol{\theta}} \left\| \boldsymbol{\varepsilon}_m(\boldsymbol{\theta}) \right\|^2 \tag{13}$$

For performing each of these minimization and fitting tasks, the built-in optimizer fmincon was used in conjunction with the nonlinear system solver *fsolve* in MATLAB R2018a. To compare individual models, we calculated the BIC according to Equation (10) where the model with the lowest BIC value best describes the reported data.

Results & Discussion:

Experimental data point strongly to the mechanism of CO_2 reduction on Au involving rate-limiting charge transfer to initiate CO_2 electrosorption.[37,53,61] Within this mechanistic framework, we compare the ability of five electrochemical models to explain the existence of curvature in Tafel plots for the conversion of CO_2 to CO. Specifically, we examine the conventional BV model, BV with mass transport considerations, an approximation to MHC, and film-resistance-modified versions of BV and MHC. The BV model is fit for the overall reaction, agnostic to the mechanistic details, whereas the MHC model makes only the implicit assumption that a single electron charge transfer limits the rate. To qualitatively contrast the models, we estimate their goodness of fit to the experimental data, analyzing their ability to capture functional form through residual analysis and evaluating their fitting parameters. Then, we quantitatively contrast the models using the BIC metric, and subsequently normalize the experimental data by either the exchange current density

or kinetic prefactor. Finally, we show the impact that incorrect electrochemical kinetic models may have on predicted economic performance of CO_2 reduction chemistry.

Butler-Volmer Kinetics and Mass-Transfer Deviations

Using the fitting methodology described above, the selected data sets (**Table 1**) were fit to the BV kinetics, as shown in Figure S1. This fitting clearly demonstrates model-data mismatch between the effectively linear BV model, and the curved Tafel data, as seen by residual analysis (Figure S2) with under-prediction of reaction rates in the intermediate region and over-prediction at extrema. Clearly, the trend observed in these residuals indicates an incompleteness with the BV model for describing CO_2 reduction. Expanding on the results of the curve fitting, we examined differences in the physically important fitting parameters. In the model, the exchange current density (Figure S3) acts as a scale factor to account for, amongst other things, different active surface areas but does not change the physical behavior, whereas the charge transfer coefficient only changes as a function of reaction chemistry. From the best fits, the charge transfer coefficient is 0.17 ± 0.07. While this value is close to the predicted transfer coefficient of 0.25 for a rate-controlling single electron exchange within a net two electron reaction,[90] this BV model cannot reconcile the large variation in values or the aforementioned trend in the residuals.

As described in the introduction, mass transport limitations may cause curvature in the Tafel plots that convolute extraction of kinetic parameters. The best fits for the BV model with mass transport (BV + MT) are shown in Figure 2a. At low overpotentials, the mass transport plays an insignificant role (i.e. $\eta_{MT} \approx 0$), and the model displays linear Tafel behavior similar to an unmodified BV; however, as overpotential increases, there exists sharp curvature followed by a plateau corresponding to the diffusion-limited current density. Assuming standard temperature and pressure, the concentration of dissolved CO_2 in aqueous electrolyte is < 35 mM and the diffusion

coefficient is ca. 1.6×10^{-5} cm^2 s^{-1}.[91] The mass-transport-governed-limiting-current-density can be calculated through Equation (14) where L_{BL} is the thickness of the boundary layer over which the CO_2 must diffuse, D is the diffusion coefficient, and C_{Bulk} is the concentration of CO_2 dissolved in the bulk electrolyte solution. A plot of limiting current density as a function of boundary layer thickness is shown in Figure S4. For reference, boundary layers of 10, 50, and 100 μm enable limiting current densities of ≈ 110, 20, and 10 mA cm^{-2}, respectively. Experimental boundary layers for planar electrodes have been measured to be ca. 70 μm[92] and order of magnitude estimates place the boundary layer thickness ca. 100 μm.[54,93]

$$j_{lim} = nFD\frac{C_{Bulk}}{L_{BL}} \tag{14}$$

Due to the fitting procedure minimizing residuals without mass transport-informed constraints, some data sets contain individual data points exceeding the best-fit limiting current density. However, any additional constraints on optimization would result in lower quality fits and larger residuals than those shown in Figure S5. Regardless, the radius of curvature during the transition between kinetic and mass transfer control in the fitted result is much smaller than that of the experimental Tafel data and demonstrates, at least qualitatively, the inability of the model to fit the data accurately, although it represents an improvement over unmodified BV kinetics.

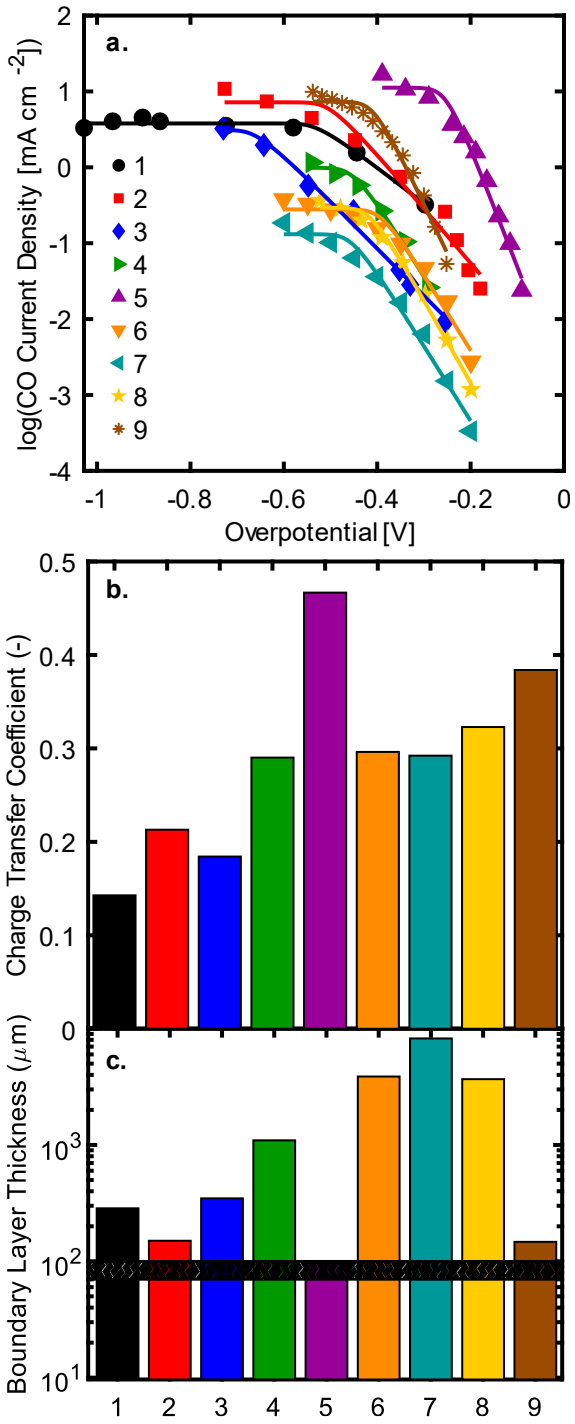

Figure 2: Analysis of the BV model with mass transport consideration showing the (a) best-fit curves overlaid on the experimental data, (b) charge transfer coefficients, and (c) boundary layer

thickness corresponding to the limiting current density, where the shaded area shows physically relevant regions.

The best-fit charge transfer coefficients span more than 30% of the allowed range between 0 and 1, indicating that a single physical value does not describe all the data sets despite the shared underlying chemistry. Similarly, the fitted limiting current densities span almost two orders of magnitude, translating to the large variations of boundary layer thicknesses observed in Figure 3c. Concerningly, the majority of the fitted boundary layer thicknesses exceed 100 μm in length, which is likely the largest dimension that gas might diffuse across a liquid interface in a porous electrolyte. Meanwhile, the largest boundary layers suggested by this analysis approach a centimeter in length, which is largely outside the realm of possibility for the physical systems. Indeed, given the similarities in curvature despite orders of magnitude differences in experimental current density and fitting parameters, it is unlikely that such curvature could be attributed to mass transfer alone.

Marcus-Hush-Chidsey Kinetics

As discussed in the introduction, the MHC kinetic model can account for Tafel plot curvature without invoking mass transfer or film resistance artifacts. The MHC fits shown in Figure 3a closely approximate the experimental data due to their inherent curvature, giving rise to well-distributed residuals (Figure S7). The kinetic prefactor (Figure S8), which is related to the maximum attainable current density at large absolute overpotentials ($|\eta| \rightarrow \infty$) spans several orders of magnitude which, again, may be reasonable given changes in active catalyst area. The calculated reorganization energies, the energy required to distort the solvation shell to a non-equilibrium configuration, all fall in the range of 1.0 ± 0.2 eV. As noted above, the overpotentials in the MHC

fits were calculated based on the equilibrium potential for the *overall* reaction, not the elementary step controlling the MHC rate. Thus, we expect that the extracted reorganization energies are offset by some unknown scalar value depending on the actual equilibrium potential of the elementary step in question. Indeed, perhaps reflecting this scalar offset, the optimized reorganization energies we find are slightly higher than the 0.75 eV value extracted recently from fitting both the equilibrium potential and reorganization energy for the elementary CO_2 reduction step to a Marcus-Hush-Levich model.[83] Nonetheless, the good fit of MHC kinetic model to the experimental data bolsters the validity of this formalism relative to a BV model for CO_2 reduction on Au.

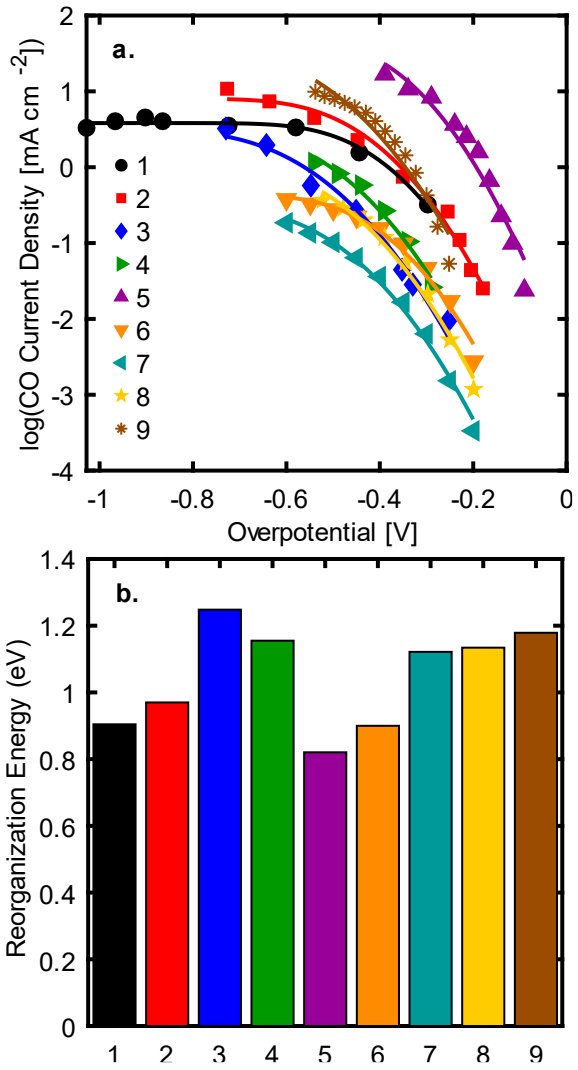

Figure 3: MHC analysis showing the (a) best-fit curves overlaid on the experimental data and (b) reorganization energies extracted from the fits.

Series Resistance Modification to BV and MHC

The BV + R and MHC + R model fits are shown in Figure S9, respectively, and show good qualitative agreement with the experimental data; however, the parameters that govern form, in this case the charge transfer coefficient (Figure S9c), reorganization energy (Figure S9d), and film resistances (Figure S9e and Figure S9f), display large variation that is likely indicative of over-

fitting. Specifically, the charge transfer coefficients for the BV + R model range from 0.2 to 0.8, demonstrating little agreement or consistency between the data sets, again despite shared fundamental process chemistry. Similarly, the reorganization energies for the MHC + R model range from 1.2 to 3.3, a significantly larger range than the best-fit values from the MHC model alone. Interestingly, the film resistances for both models are similar (10^1-10^3 Ω cm^2) and match the order of magnitude of prior reports, suggesting that this component dominates the fit. However, ascribing physical meaning to these film resistance values is difficult as no corroborating evidence of passivating film development has been presented in the CO_2 reduction literature and the mechanism by which such a film might form is unclear in an aqueous electrolyte solution under reducing conditions.

Quantitative Model Comparison

Thus far, goodness of fit and model comparison has been qualitative and based largely on the feasibility of the best fit parameters. Accordingly, we calculated the BIC metric to quantify the accuracy and predictive capability of the different models under investigation (BV, MHC, BV + MT, BV + R, MHC + R). As described in the Methods section (*vide supra*), a lower BIC indicates greater veracity of the model. The BIC values are shown for the individual data sets 1-9 that have been fitted throughout the manuscript, and for each individual model that they were fit to, in Figure 4. In these data, the BIC for the MHC model is consistently lower than that of any other tested model. Despite the limited data in each individual set ($7 < N < 14$), the aggregate strengthens the conclusion of MHC being a more likely model than any of the others examined.

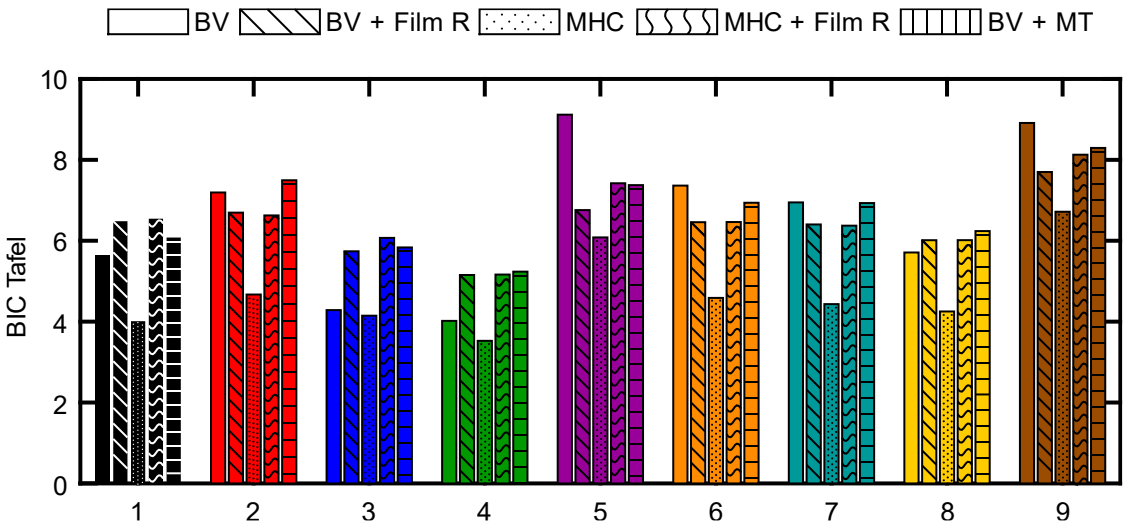

Figure 4: Computed BIC for each of the representative data sets presented, comparing the different models, where a low BIC corresponds to a higher model veracity.

As all the data harvested within this manuscript are of the same reaction, on the same catalyst, with similar electrolyte solutions, but varying in catalyst morphology (e.g., surface area), there should be shared fundamental behavior that underlies all data sets. Therefore, given the apparent applicability of the MHC model as shown above, we anticipate an ability to collapse the disparate data sets onto a governing curve by an appropriate scaling of the relevant parameters. To evaluate this hypothesis, we define a normalized current, which is the ratio of the measured current to the best-fit maximum achievable current obtained from the MHC model, shown in Equation 16, below.

$$\tilde{j} = \frac{j_{meas}}{2k_0\sqrt{\pi\lambda}} \tag{15}$$

The effect of this normalization is seen below, in Figure **5**, where the data sets collapse in a window spanning about 0.5 decades on the Tafel plot likely due to convolutions between imprecise experimental measurements and nonzero confidence intervals surrounding the fitted parameters.

Additionally, to increase the credibility of the analysis, we incorporated alternate (alt) Au data sets from the literature in the figure.[28,50,51] The MHC model superiority can be further supported by showing the inability of the remaining models to collapse the data with their model-specific fitted current scales (Figures S15-S18), and best-fit film resistances that lie well outside the range of any reasonably explainable value (Figures S19 and S20).

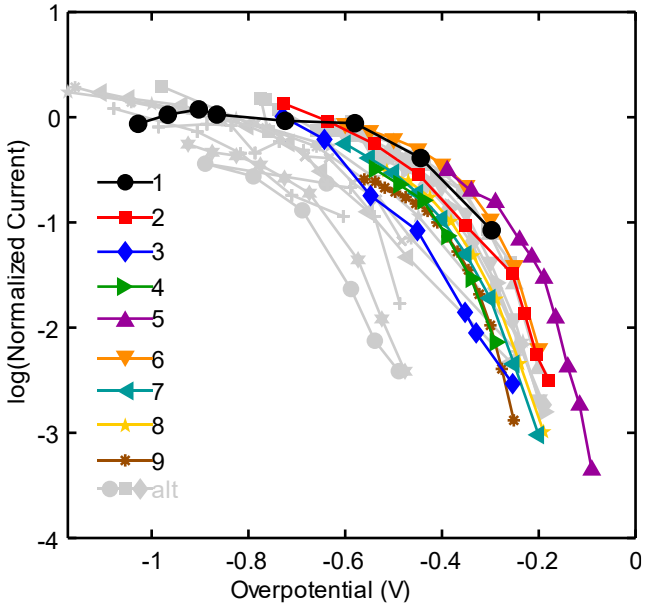

Figure 5: Normalized data sets that are aggregated into a single set for model fitting and comparison.

To demonstrate the possible impact of model selection on electrochemical engineering design, we consider the techno-economic model that was previously developed by one of the authors, leveraging the BV model.[94] Based on this original analysis, the cost to the consumer is highly sensitive to the applied current density. Given the low cost of electricity compared to the high price of capital equipment, the minimal production cost is achieved when the current density is nearly the limiting current density achieved by mass transfer to the surface. However, the analysis presented in this manuscript suggests that a kinetically limited current exists below the mass-

transfer limiting current for the reduction of CO_2 to CO, indicating that the true minimum cost may be orders of magnitude different than originally predicted. In Figure 6 we show the minimum cost of CO produced by CO_2 reduction as a function of the MHC limiting current density, $2k_0(\pi\lambda)^{1/2}$, obtained using $\lambda = 1$ eV while varying k_0, compared to the minimum cost obtained at the mass-transfer limiting current density of ca. 500 mA cm^{-2} used in the original manuscript by Orella et al.[94] Clearly, to have an accurate sense of the techno-economic promise of electrochemical upgrading schemes, the correct electrochemical kinetic model is a necessary component. To that end, it is imperative that researchers investigating the plethora of electrochemical upgrading schemes of interest begin considering alternative electrochemical kinetic descriptors in both their experimental and modeling efforts.

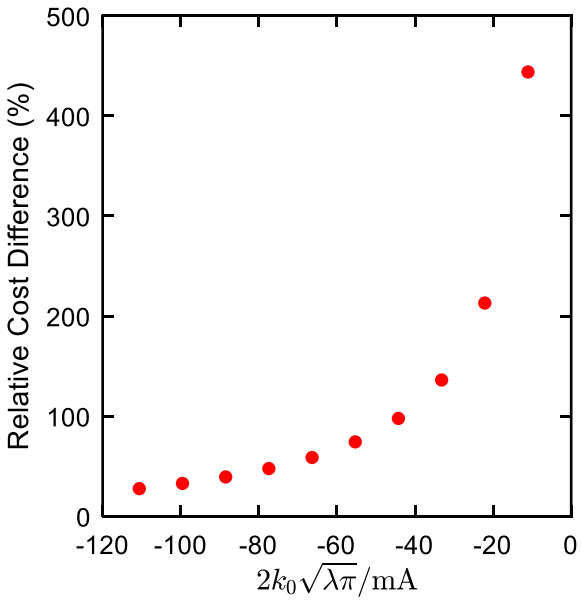

Figure 6: Difference between the estimated cost of CO production when using the BV model and an MHC model with varying maximum currents, with a mass-transfer limited current of ca. 500 mA cm^{-2}. As the maximum attainable kinetic current approaches the mass-transfer limited current, the deviation between the two models is vanishingly small.

Conclusions:

In summary, this work fit a variety of electrochemical models to a survey of experimental literature data on Au catalysts to gain insight into the kinetics of CO_2 reduction to CO. First, we motivated the need for accurate electrokinetic models to advance techno-economic feasibility analyses and inform operational process decisions. Then, we analyzed BV- and MHC- based models, including some with modifications to account for mass transport or series resistance during charge transfer, to qualitatively capture the functional form of the data with reasonable fitting parameters. Unmodified MHC kinetic theory was the only model to exhibit a consistent set of fitting parameters while also achieving a fit that visually agreed with the data. The validity of this model was strengthened by the results of a goodness of fit analysis, using Bayesian statistics that penalize overfitting, which determined that MHC kinetic theory was the model that was most likely to describe the data for every data set. Further, we normalized each data set by the kinetic prefactor from the MHC fitting, to account for differences in electrode morphology, and the data collapsed onto a single curve. Finally, we showed the financial impact that incorrect kinetic modeling may have on the economics of CO_2 electrolysis. Overall, these results indicate that a Marcus formalism[77–80] provides both a more accurate and a more physically informative picture than Butler-Volmer kinetics for CO_2 reduction to CO. Lastly, we hope that these results inspire greater use of the MHC kinetic theory (in its simple analytical forms[58,82]) to describe the CO_2 reduction reaction and motivate a renewed interest in developing and applying more rigorous models of inner-sphere charge transfer reactions that underlie important energy conversion reactions

Acknowledgements:

We gratefully acknowledge funding through a Shell-MITEI Member Energy Research Fund. As a part of this collaboration, the authors would like to thank Elizabeth Endler and Albert Harvey from Shell for insightful discussions and research suggestions. Also, the authors thank McLain Leonard, Connor Coley, Michael McEldrew, and Dimitrios Fraggedakis for discussions regarding kinetic theory and statistical analysis. Yogesh Surendranath acknowledges the Air Force Office of Scientific Research (AFOSR) under Award Number FA9550-18-1-0420.

Glossary of Terms:

j	Geometric current density	A cm^{-2}
j_0	Exchange current density	A cm^{-2}
α	Charge transfer coefficient	
η	Overpotential	V
$\tilde{\eta}$	Dimensionless overpotential	
n	Number of electrons	
F	Faraday constant	C mol^{-1}
R	Ideal gas constant	J mol^{-1} K^{-1}
T	Temperature	K
$\tilde{\eta}_K$	Dimensionless kinetic overpotential	
$\tilde{\eta}_T$	Dimensionless mass transport overpotential	
j_{lim}	Limiting geometric current density	A cm^{-2}
k_0	Kinetic prefactor	A cm^{-2}
λ	Reorganization energy	eV
R_{int}	Internal resistance	Ω cm^2
$\hat{j}$	Conduction current	Ω^{-1} cm^{-2}
p	Probability density	
m	Model	
d	Data	
$\boldsymbol{\theta}$	Model parameters	
$\boldsymbol{\theta}^*$	Best fit model parameters	
B_{ij}	Bayes factor	
N	Number of data points	
k	Degree of model	
$\mathcal{L}$	Likelihood function	
$\boldsymbol{\varepsilon}$	Residuals for model m	
σ^2	Variance in collected data	
D	Diffusion coefficient	m^2 s^{-1}
C_{Bulk}	Bulk concentration	mol m^{-3}

L_{BL}	Boundary layer thickness	m
e	Electron charge	C

Supporting Information

Additional analysis of kinetic data using the models described in the main text. Parallel workup of silver catalyst data.

References

(1) Peter, S. C. Reduction of CO2 to Chemicals and Fuels: A Solution to Global Warming and Energy Crisis. *ACS Energy Lett.* **2018**, *3* (7), 1557–1561. https://doi.org/10.1021/acsenergylett.8b00878.

(2) Kenis, P. J. A.; Dibenedetto, A.; Zhang, T. Carbon Dioxide Utilization Coming of Age. *ChemPhysChem* **2017**. https://doi.org/10.1002/cphc.201701204.

(3) Yuan, Z.; Eden, M. R.; Gani, R. Toward the Development and Deployment of Large-Scale Carbon Dioxide Capture and Conversion Processes. *Ind. Eng. Chem. Res.* **2016**, *55* (12), 3383–3419. https://doi.org/10.1021/acs.iecr.5b03277.

(4) Majumdar, A.; Deutch, J. Research Opportunities for CO2 Utilization and Negative Emissions at the Gigatonne Scale. *Joule* **2018**, *2* (5), 805–809. https://doi.org/10.1016/j.joule.2018.04.018.

(5) Chen, Y.; Lewis, N. S.; Xiang, C. Operational Constraints and Strategies for Systems to Effect the Sustainable, Solar-Driven Reduction of Atmospheric CO $_2$. *Energy Env. Sci* **2015**, *8* (12), 3663–3674. https://doi.org/10.1039/C5EE02908B.

(6) Bruckner, T. Decarbonizing the Global Energy System: An Updated Summary of the IPCC Report on Mitigating Climate Change. *Energy Technol.* **2016**, *4* (1), 19–30. https://doi.org/10.1002/ente.201500387.

(7) Lu, Q.; Rosen, J.; Jiao, F. Nanostructured Metallic Electrocatalysts for Carbon Dioxide Reduction. *ChemCatChem* **2015**, *7* (1), 38–47. https://doi.org/10.1002/cctc.201402669.

(8) Hori, Y.; Wakebe, H.; Tsukamoto, T.; Koga, O. Electrocatalytic Process of CO Selectivity in Electrochemical Reduction of CO2 at Metal Electrodes in Aqueous Media. *Electrochimica Acta* **1994**, *39* (11–12), 1833–1839. https://doi.org/10.1016/0013-4686(94)85172-7.

(9) Kuhl, K. P.; Cave, E. R.; Abram, D. N.; Jaramillo, T. F. New Insights into the Electrochemical Reduction of Carbon Dioxide on Metallic Copper Surfaces. *Energy Environ. Sci.* **2012**, *5* (5), 7050–7059. https://doi.org/10.1039/C2EE21234J.

(10) Sen, S.; Liu, D.; Palmore, G. T. R. Electrochemical Reduction of CO2 at Copper Nanofoams. *ACS Catal.* **2014**, *4* (9), 3091–3095. https://doi.org/10.1021/cs500522g.

(11) Sen, S.; Skinn, B.; Hall, T.; Inman, M.; Taylor, E. J.; Brushett, F. R. Pulsed Electrodeposition of Tin Electrocatalysts onto Gas Diffusion Layers for Carbon Dioxide Reduction to Formate. *MRS Adv.* **2017**, *2* (8), 451–458. https://doi.org/10.1557/adv.2016.652.

(12) Kopljar, D.; Inan, A.; Vindayer, P.; Wagner, N.; Klemm, E. Electrochemical Reduction of CO2 to Formate at High Current Density Using Gas Diffusion Electrodes. *J. Appl. Electrochem.* **2014**, *44* (10), 1107–1116. https://doi.org/10.1007/s10800-014-0731-x.

(13) Yang, H.; Kaczur, J. J.; Sajjad, S. D.; Masel, R. I. Electrochemical Conversion of CO 2 to Formic Acid Utilizing Sustainion™ Membranes. *J. CO2 Util.* **2017**, *20*, 208–217. https://doi.org/10.1016/j.jcou.2017.04.011.

(14) Rosen, J.; Hutchings, G. S.; Lu, Q.; Rivera, S.; Zhou, Y.; Vlachos, D. G.; Jiao, F. Mechanistic Insights into the Electrochemical Reduction of CO_2 to CO on Nanostructured Ag Surfaces. *ACS Catal.* **2015**, *5* (7), 4293–4299. https://doi.org/10.1021/acscatal.5b00840.

(15) Rosen, B. A.; Salehi-Khojin, A.; Thorson, M. R.; Zhu, W.; Whipple, D. T.; Kenis, P. J. A.; Masel, R. I. Ionic Liquid–Mediated Selective Conversion of CO2 to CO at Low Overpotentials. *Science* **2011**, *334* (6056), 643–644. https://doi.org/10.1126/science.1209786.

(16) Jhong, H.-R. "Molly"; Tornow, C. E.; Kim, C.; Verma, S.; Oberst, J. L.; Anderson, P. S.; Gewirth, A. A.; Fujigaya, T.; Nakashima, N.; Kenis, P. J. A. Gold Nanoparticles on Polymer-Wrapped Carbon Nanotubes: An Efficient and Selective Catalyst for the Electroreduction of CO2. *ChemPhysChem* n/a-n/a. https://doi.org/10.1002/cphc.201700815.

(17) Ma, S.; Luo, R.; Gold, J. I.; Yu, A. Z.; Kim, B.; Kenis, P. J. A. Carbon Nanotube Containing Ag Catalyst Layers for Efficient and Selective Reduction of Carbon Dioxide. *J. Mater. Chem. A* **2016**, *4* (22), 8573–8578. https://doi.org/10.1039/C6TA00427J.

(18) Lu, Q.; Rosen, J.; Zhou, Y.; Hutchings, G. S.; Kimmel, Y. C.; Chen, J. G.; Jiao, F. A Selective and Efficient Electrocatalyst for Carbon Dioxide Reduction. *Nat. Commun.* **2014**, *5*, 3242. https://doi.org/10.1038/ncomms4242.

(19) Kuhl, K. P.; Hatsukade, T.; Cave, E. R.; Abram, D. N.; Kibsgaard, J.; Jaramillo, T. F. Electrocatalytic Conversion of Carbon Dioxide to Methane and Methanol on Transition Metal Surfaces. *J. Am. Chem. Soc.* **2014**, *136* (40), 14107–14113. https://doi.org/10.1021/ja505791r.

(20) Varela, A. S.; Kroschel, M.; Reier, T.; Strasser, P. Controlling the Selectivity of CO2 Electroreduction on Copper: The Effect of the Electrolyte Concentration and the Importance of the Local PH. *Catal. Today* **2016**, *260*, 8–13. https://doi.org/10.1016/j.cattod.2015.06.009.

(21) Cook, R. L.; MacDuff, R. C.; Sammells, A. F. High Rate Gas Phase CO 2 Reduction to Ethylene and Methane Using Gas Diffusion Electrodes. *J. Electrochem. Soc.* **1990**, *137* (2), 607–608. https://doi.org/10.1149/1.2086515.

(22) Tang, W.; A. Peterson, A.; Sofia Varela, A.; P. Jovanov, Z.; Bech, L.; J. Durand, W.; Dahl, S.; K. Nørskov, J.; Chorkendorff, I. The Importance of Surface Morphology in Controlling the Selectivity of Polycrystalline Copper for CO2 Electroreduction. *Phys. Chem. Chem. Phys.* **2012**, *14* (1), 76–81. https://doi.org/10.1039/C1CP22700A.

(23) Reske, R.; Mistry, H.; Behafarid, F.; Roldan Cuenya, B.; Strasser, P. Particle Size Effects in the Catalytic Electroreduction of CO2 on Cu Nanoparticles. *J. Am. Chem. Soc.* **2014**, *136* (19), 6978–6986. https://doi.org/10.1021/ja500328k.

(24) Riduan, S. N.; Zhang, Y.; Ying, J. Y. Conversion of Carbon Dioxide into Methanol with Silanes over N-Heterocyclic Carbene Catalysts. *Angew. Chem.* **2009**, *121* (18), 3372–3375. https://doi.org/10.1002/ange.200806058.

(25) Rodriguez, J. A.; Liu, P.; Stacchiola, D. J.; Senanayake, S. D.; White, M. G.; Chen, J. G. Hydrogenation of CO2 to Methanol: Importance of Metal–Oxide and Metal–Carbide Interfaces in the Activation of CO2. *ACS Catal.* **2015**, *5* (11), 6696–6706. https://doi.org/10.1021/acscatal.5b01755.

(26) Wu, J.; Ma, S.; Sun, J.; Gold, J. I.; Tiwary, C.; Kim, B.; Zhu, L.; Chopra, N.; Odeh, I. N.; Vajtai, R.; Yu, A. Z.; Luo, R.; Lou, J.; Ding, G.; Kenis, P. J. A.; Ajayan, P. M. A Metal-Free Electrocatalyst for Carbon Dioxide Reduction to Multi-Carbon Hydrocarbons and Oxygenates. *Nat. Commun.* **2016**, *7*. https://doi.org/10.1038/ncomms13869.

(27) Li, C. W.; Ciston, J.; Kanan, M. W. Electroreduction of Carbon Monoxide to Liquid Fuel on Oxide-Derived Nanocrystalline Copper. *Nature* **2014**, *508* (7497), 504–507. https://doi.org/10.1038/nature13249.

(28) Hori, Y.; Murata, A.; Kikuchi, K.; Suzuki, S. Electrochemical Reduction of Carbon Dioxides to Carbon Monoxide at a Gold Electrode in Aqueous Potassium Hydrogen Carbonate. *J. Chem. Soc. Chem. Commun.* **1987**, No. 10, 728–729. https://doi.org/10.1039/C39870000728.

(29) Koppenol, W. H.; Rush, J. D. Reduction Potential of the Carbon Dioxide/Carbon Dioxide Radical Anion: A Comparison with Other C1 Radicals. *J. Phys. Chem.* **1987**, *91* (16), 4429–4430.

(30) Amatore, C.; Saveant, J. M. Mechanism and Kinetic Characteristics of the Electrochemical Reduction of Carbon Dioxide in Media of Low Proton Availability. *J. Am. Chem. Soc.* **1981**, *103* (17), 5021–5023.

(31) Noda, H.; Ikeda, S.; Yamamoto, A.; Einaga, H.; Ito, K. Kinetics of Electrochemical Reduction of Carbon Dioxide on a Gold Electrode in Phosphate Buffer Solutions. *Bull. Chem. Soc. Jpn.* **1995**, *68* (7), 1889–1895. https://doi.org/10.1246/bcsj.68.1889.

(32) Zhu, W.; Michalsky, R.; Metin, Ö.; Lv, H.; Guo, S.; Wright, C. J.; Sun, X.; Peterson, A. A.; Sun, S. Monodisperse Au Nanoparticles for Selective Electrocatalytic Reduction of CO2 to CO. *J. Am. Chem. Soc.* **2013**, *135* (45), 16833–16836. https://doi.org/10.1021/ja409445p.

(33) Feaster, J. T.; Shi, C.; Cave, E. R.; Hatsukade, T.; Abram, D. N.; Kuhl, K. P.; Hahn, C.; Nørskov, J. K.; Jaramillo, T. F. Understanding Selectivity for the Electrochemical Reduction of Carbon Dioxide to Formic Acid and Carbon Monoxide on Metal Electrodes. *ACS Catal.* **2017**, 4822–4827. https://doi.org/10.1021/acscatal.7b00687.

(34) Chen, L. D.; Urushihara, M.; Chan, K.; Nørskov, J. K. Electric Field Effects in Electrochemical CO2 Reduction. *ACS Catal.* **2016**, *6* (10), 7133–7139. https://doi.org/10.1021/acscatal.6b02299.

(35) Zhu, W.; Zhang, Y.-J.; Zhang, H.; Lv, H.; Li, Q.; Michalsky, R.; Peterson, A. A.; Sun, S. Active and Selective Conversion of CO2 to CO on Ultrathin Au Nanowires. *J. Am. Chem. Soc.* **2014**, *136* (46), 16132–16135. https://doi.org/10.1021/ja5095099.

(36) Peterson, A. A.; Abild-Pedersen, F.; Studt, F.; Rossmeisl, J.; Nørskov, J. K. How Copper Catalyzes the Electroreduction of Carbon Dioxide into Hydrocarbon Fuels. *Energy Environ. Sci.* **2010**, *3* (9), 1311–1315. https://doi.org/10.1039/C0EE00071J.

(37) Wuttig, A.; Yaguchi, M.; Motobayashi, K.; Osawa, M.; Surendranath, Y. Inhibited Proton Transfer Enhances Au-Catalyzed CO2-to-Fuels Selectivity. *Proc. Natl. Acad. Sci.* **2016**, *113* (32), E4585–E4593. https://doi.org/10.1073/pnas.1602984113.

(38) Chernyshova, I. V.; Somasundaran, P.; Ponnurangam, S. On the Origin of the Elusive First Intermediate of CO2 Electroreduction. *Proc. Natl. Acad. Sci.* **2018**, 201802256. https://doi.org/10.1073/pnas.1802256115.

(39) Ringe, S.; Morales-Guio, C. G.; Chen, L. D.; Fields, M.; Jaramillo, T. F.; Hahn, C.; Chan, K. Double Layer Charging Driven Carbon Dioxide Adsorption Limits the Rate of Electrochemical Carbon Dioxide Reduction on Gold. *Nat. Commun.* **2020**, *11* (1), 1–11. https://doi.org/10.1038/s41467-019-13777-z.

(40) Bazant, M. Z. Theory of Chemical Kinetics and Charge Transfer Based on Nonequilibrium Thermodynamics. *Acc. Chem. Res.* **2013**, *46* (5), 1144–1160. https://doi.org/10.1021/ar300145c.

(41) Chidsey, C. E. D. Free Energy and Temperature Dependence of Electron Transfer at the Metal-Electrolyte Interface. *Science* **1991**, *251* (4996), 919–922. https://doi.org/10.1126/science.251.4996.919.

(42) Henstridge, M. C.; Laborda, E.; Rees, N. V.; Compton, R. G. Marcus–Hush–Chidsey Theory of Electron Transfer Applied to Voltammetry: A Review. *Electrochimica Acta* **2012**, *84*, 12–20. https://doi.org/10.1016/j.electacta.2011.10.026.

(43) Latz, A.; Zausch, J. Thermodynamic Derivation of a Butler–Volmer Model for Intercalation in Li-Ion Batteries. *Electrochimica Acta* **2013**, *110*, 358–362. https://doi.org/10.1016/j.electacta.2013.06.043.

(44) Brown, S. M.; Hsiao, Y. W.; Orella, M. J.; Brushett, F. R. Electrode Characterization in a Flowing Electrolyte Reactor for the Electrochemical Reduction of CO2 to CO. *Meet. Abstr.* **2017**, *MA2017-02* (45), 2001–2001.

(45) Brown, S. M.; Kim, C.; Hsiao, Y. W.; Salih, T. K.; Bumajdad, A.; Brushett, F. R. Impact of Catalyst Support on Activity and Selectivity of Gold Nanoparticles for the Carbon Dioxide Reduction Reaction. *Meet. Abstr.* **2016**, *MA2016-01* (35), 1787–1787.

(46) Salih, T.; Brown, S. M.; Kim, C.; Carroll, K. J.; Brushett, F. R.; Bumajdad, A. Cost Effective and Scalable Synthesis of Supported Au Nanoparticles for the Electroreduction of CO2 to CO. *Sci. Adv. Mater.* **2017**, *9* (6), 888–895. https://doi.org/10.1166/sam.2017.3019.

(47) Cave, E. R.; Montoya, J. H.; Kuhl, K. P.; Abram, D. N.; Hatsukade, T.; Shi, C.; Hahn, C.; Nørskov, J. K.; Jaramillo, T. F. Electrochemical CO2 Reduction on Au Surfaces: Mechanistic Aspects Regarding the Formation of Major and Minor Products. *Phys. Chem. Chem. Phys.* **2017**. https://doi.org/10.1039/C7CP02855E.

(48) Cao, Z.; Kim, D.; Hong, D.; Yu, Y.; Xu, J.; Lin, S.; Wen, X.; Nichols, E. M.; Jeong, K.; Reimer, J. A.; Yang, P.; Chang, C. J. A Molecular Surface Functionalization Approach to Tuning Nanoparticle Electrocatalysts for Carbon Dioxide Reduction. *J. Am. Chem. Soc.* **2016**, *138* (26), 8120–8125. https://doi.org/10.1021/jacs.6b02878.

(49) Chen, Y.; Li, C. W.; Kanan, M. W. Aqueous CO2 Reduction at Very Low Overpotential on Oxide-Derived Au Nanoparticles. *J. Am. Chem. Soc.* **2012**, *134* (49), 19969–19972. https://doi.org/10.1021/ja309317u.

(50) Feng, X.; Jiang, K.; Fan, S.; Kanan, M. W. Grain-Boundary-Dependent CO2 Electroreduction Activity. *J. Am. Chem. Soc.* **2015**, *137* (14), 4606–4609. https://doi.org/10.1021/ja5130513.

(51) Hall, A. S.; Yoon, Y.; Wuttig, A.; Surendranath, Y. Mesostructure-Induced Selectivity in CO2 Reduction Catalysis. *J. Am. Chem. Soc.* **2015**, *137* (47), 14834–14837. https://doi.org/10.1021/jacs.5b08259.

(52) Arora, P.; Doyle, M.; White, R. E. Mathematical Modeling of the Lithium Deposition Overcharge Reaction in Lithium-Ion Batteries Using Carbon-Based Negative Electrodes. *J. Electrochem. Soc.* **1999**, *146* (10), 3543–3553. https://doi.org/10.1149/1.1392512.

(53) Zhang, B. A.; Ozel, T.; Elias, J. S.; Costentin, C.; Nocera, D. G. Interplay of Homogeneous Reactions, Mass Transport, and Kinetics in Determining Selectivity of the Reduction of CO2 on Gold Electrodes. *ACS Cent. Sci.* **2019**, *5* (6), 1097–1105. https://doi.org/10.1021/acscentsci.9b00302.

(54) Lobaccaro, P.; Singh, M. R.; Clark, E. L.; Kwon, Y.; Bell, A. T.; Ager, J. W. Effects of Temperature and Gas–Liquid Mass Transfer on the Operation of Small Electrochemical Cells for the Quantitative Evaluation of CO_2 Reduction Electrocatalysts. *Phys Chem Chem Phys* **2016**, *18* (38), 26777–26785. https://doi.org/10.1039/C6CP05287H.

(55) Doyle, M.; Newman, J.; Gozdz, A. S.; Schmutz, C. N.; Tarascon, J.-M. Comparison of Modeling Predictions with Experimental Data from Plastic Lithium Ion Cells. *J. Electrochem. Soc.* **1996**, *143* (6), 1890–1903. https://doi.org/10.1149/1.1836921.

(56) Darcovich, K.; Kenney, B.; MacNeil, D. D.; Armstrong, M. M. Control Strategies and Cycling Demands for Li-Ion Storage Batteries in Residential Micro-Cogeneration Systems. *Appl. Energy* **2015**, *141*, 32–41. https://doi.org/10.1016/j.apenergy.2014.11.079.

(57) Thomas-Alyea, K. E.; Jung, C.; Smith, R. B.; Bazant, M. Z. In Situ Observation and Mathematical Modeling of Lithium Distribution within Graphite. *J. Electrochem. Soc.* **2017**, *164* (11), E3063. https://doi.org/10.1149/2.0061711jes.

(58) Zeng, Y.; Smith, R. B.; Bai, P.; Bazant, M. Z. Simple Formula for Marcus–Hush–Chidsey Kinetics. *J. Electroanal. Chem.* **2014**, *735*, 77–83. https://doi.org/10.1016/j.jelechem.2014.09.038.

(59) Smith, R. B.; Bazant, M. Z. Multiphase Porous Electrode Theory. *J. Electrochem. Soc.* **2017**, *164* (11), E3291–E3310. https://doi.org/10.1149/2.0171711jes.

(60) Fraggedakis, D.; McEldrew, M.; Smith, R. B.; Krishnan, Y.; Zhang, Y.; Chueh, W.; Bai, P.; Shao-Horn, Y.; Bazant, M. Z. Theory of Coupled Ion-Electron Transfer Kinetics.

(61) Wuttig, A.; Yoon, Y.; Ryu, J.; Surendranath, Y. Bicarbonate Is Not a General Acid in Au-Catalyzed CO2 Electroreduction. *J. Am. Chem. Soc.* **2017**, *139* (47), 17109–17113. https://doi.org/10.1021/jacs.7b08345.

(62) Hsieh, Y.-C.; Senanayake, S. D.; Zhang, Y.; Xu, W.; Polyansky, D. E. Effect of Chloride Anions on the Synthesis and Enhanced Catalytic Activity of Silver Nanocoral Electrodes for CO $_2$ Electroreduction. *ACS Catal.* **2015**, *5* (9), 5349–5356. https://doi.org/10.1021/acscatal.5b01235.

(63) Jiang, K.; Kharel, P.; Peng, Y.; Gangishetty, M. K.; Lin, H.-Y. G.; Stavitski, E.; Attenkofer, K.; Wang, H. Silver Nanoparticles with Surface-Bonded Oxygen for Highly Selective CO $_2$ Reduction. *ACS Sustain. Chem. Eng.* **2017**, *5* (10), 8529–8534. https://doi.org/10.1021/acssuschemeng.7b02380.

(64) Ma, S.; Liu, J.; Sasaki, K.; Lyth, S. M.; Kenis, P. J. A. Carbon Foam Decorated with Silver Nanoparticles for Electrochemical CO $_2$ Conversion. *Energy Technol.* **2017**, *5* (6), 861–863. https://doi.org/10.1002/ente.201600576.

(65) Hatsukade, T.; Kuhl, K. P.; Cave, E. R.; Abram, D. N.; Jaramillo, T. F. Insights into the Electrocatalytic Reduction of CO $_2$ on Metallic Silver Surfaces. *Phys Chem Chem Phys* **2014**, *16* (27), 13814–13819. https://doi.org/10.1039/C4CP00692E.

(66) Verma, S.; Lu, X.; Ma, S.; Masel, R. I.; Kenis, P. J. A. The Effect of Electrolyte Composition on the Electroreduction of CO $_2$ to CO on Ag Based Gas Diffusion Electrodes. *Phys. Chem. Chem. Phys.* **2016**, *18* (10), 7075–7084. https://doi.org/10.1039/C5CP05665A.

(67) Marcus, R. A. On the Theory of Electrochemical and Chemical Electron Transfer Processes. *Can. J. Chem.* **1959**, *37* (1), 155–163. https://doi.org/10.1139/v59-022.

(68) Marcus, R. A. Electrostatic Free Energy and Other Properties of States Having Nonequilibrium Polarization. I. *J. Chem. Phys.* **1956**, *24* (5), 979–989. https://doi.org/10.1063/1.1742724.

(69) Marcus, R. A. On the Theory of Oxidation-Reduction Reactions Involving Electron Transfer. I. *J. Chem. Phys.* **1956**, *24* (5), 966–978. https://doi.org/10.1063/1.1742723.

(70) Hush, N. S. Adiabatic Theory of Outer Sphere Electron-Transfer Reactions in Solution. *Trans. Faraday Soc.* **1961**, *57* (0), 557–580. https://doi.org/10.1039/TF9615700557.

(71) Hush, N. S. Homogeneous and Heterogeneous Optical and Thermal Electron Transfer. *Electrochimica Acta* **1968**, *13* (5), 1005–1023. https://doi.org/10.1016/0013-4686(68)80032-5.

(72) Hush, N. S. Distance Dependence of Electron Transfer Rates. *Coord. Chem. Rev.* **1985**, *64*, 135–157. https://doi.org/10.1016/0010-8545(85)80047-3.

(73) Dogonadze, R. R.; Chizmadzhev, Y. A. The kinetics of some electrochemical redoxy reactions on metals. *Dokl Akad Nauk SSSR* **1962**, *145* (4), 849–852.

(74) Dogonadze, R. R.; Kuznetsov, A. M.; Chernenko, A. A. THEORY OF HOMOGENEOUS AND HETEROGENEOUS ELECTRONIC PROCESSES IN LIQUIDS. *Russ. Chem. Rev.* **1965**, *34* (10), 759. https://doi.org/10.1070/RC1965v034n10ABEH001561.

(75) Levich, V. G.; Dogonadze, R. R. Osnovnie Voprosi Sovremenoi Teoreticheskoi Elektrokhimii. In *14th CITCE Meeting*; 1963; p 21.

(76) Schmickler, W. A Theory of Adiabatic Electron-Transfer Reactions. *J. Electroanal. Chem. Interfacial Electrochem.* **1986**, *204* (1), 31–43. https://doi.org/10.1016/0022-0728(86)80505-8.

(77) Kuznetsov, A. M.; Ulstrup, J. *Electron Transfer in Chemistry and Biology : An Introduction to the Theory.*; Wiley, 1999.

(78) Schmickler, W.; Santos, E. *Interfacial Electrochemistry*, 2nd ed.; Springer-Verlag: Berlin Heidelberg, 2010. https://doi.org/10.1007/978-3-642-04937-8.

(79) Bard, A. J.; Faulkner, L. R. *Electrochemical Methods*, 2. ed.; Wiley: New York, 2001.

(80) Marcus, R. A. Electron Transfer Reactions in Chemistry. Theory and Experiment. *Rev. Mod. Phys.* **1993**, *65* (3), 599–610. https://doi.org/10.1103/RevModPhys.65.599.

(81) Bai, P.; Bazant, M. Z. Charge Transfer Kinetics at the Solid–Solid Interface in Porous Electrodes. *Nat. Commun.* **2014**, *5*. https://doi.org/10.1038/ncomms4585.

(82) Zeng, Y.; Bai, P.; Smith, R. B.; Bazant, M. Z. Simple Formula for Asymmetric Marcus–Hush Kinetics. *J. Electroanal. Chem.* **2015**, *748*, 52–57. https://doi.org/10.1016/j.jelechem.2015.04.018.

(83) Zhang, B. A.; Costentin, C.; Nocera, D. G. Driving Force Dependence of Inner-Sphere Electron Transfer for the Reduction of CO2 on a Gold Electrode. *J. Chem. Phys.* **2020**, *153* (9), 094701. https://doi.org/10.1063/5.0016298.

(84) Hypothesis Testing and Model Selection. In *An Introduction to Bayesian Analysis: Theory and Methods*; Ghosh, J. K., Delampady, M., Samanta, T., Eds.; Springer Texts in Statistics; Springer New York: New York, NY, 2006; pp 159–204. https://doi.org/10.1007/978-0-387-35433-0_6.

(85) Neal, R. M. Probabilistic Inference Using Markov Chain Monte Carlo Methods. 144.

(86) Altekar, G.; Dwarkadas, S.; Huelsenbeck, J. P.; Ronquist, F. Parallel Metropolis Coupled Markov Chain Monte Carlo for Bayesian Phylogenetic Inference. *Bioinformatics* **2004**, *20* (3), 407–415. https://doi.org/10.1093/bioinformatics/btg427.

(87) Stewart, L. Bayesian Analysis Using Monte Carlo Integration – a Powerful Methodology for Handling Some Difficult Problems. *J. R. Stat. Soc. Ser. Stat.* **1983**, *32* (1–2), 195–200. https://doi.org/10.2307/2987612.

(88) Bhat, H. S.; Kumar, N. On the Derivation of the Bayesian Information Criterion. 5.

(89) Bayesian Inference and Decision Theory. In *An Introduction to Bayesian Analysis: Theory and Methods*; Ghosh, J. K., Delampady, M., Samanta, T., Eds.; Springer Texts in Statistics; Springer New York: New York, NY, 2006; pp 29–63. https://doi.org/10.1007/978-0-387-35433-0_2.

(90) Khoo, E.; Bazant, M. Z. Theory of Voltammetry in Charged Porous Media. *J. Electroanal. Chem.* **2018**, *811*, 105–120. https://doi.org/10.1016/j.jelechem.2018.01.023.

(91) Cadogan, S. P.; Maitland, G. C.; Trusler, J. P. M. Diffusion Coefficients of CO2 and N2 in Water at Temperatures between 298.15 K and 423.15 K at Pressures up to 45 MPa. *J. Chem. Eng. Data* **2014**, *59* (2), 519–525. https://doi.org/10.1021/je401008s.

(92) Lum, Y.; Yue, B.; Lobaccaro, P.; Bell, A. T.; Ager, J. W. Optimizing C–C Coupling on Oxide-Derived Copper Catalysts for Electrochemical CO 2 Reduction. *J. Phys. Chem. C* **2017**, *121* (26), 14191–14203. https://doi.org/10.1021/acs.jpcc.7b03673.

(93) Monroe, M. M.; Lobaccaro, P.; Lum, Y.; Ager, J. W. Membraneless Laminar Flow Cell for Electrocatalytic CO 2 Reduction with Liquid Product Separation. *J. Phys. Appl. Phys.* **2017**, *50* (15), 154006. https://doi.org/10.1088/1361-6463/aa6359.

(94) Orella, M. J.; Brown, S. M.; Leonard, M. E.; Román-Leshkov, Y.; Brushett, F. R. A General Technoeconomic Model for Evaluating Emerging Electrolytic Processes. *Energy Technol. n/a* (n/a), 1900994. https://doi.org/10.1002/ente.201900994.